Global NEST Journal, Vol 25, No X, pp 1-8

Assessment of object-based classification for mapping land use and land cover using google earth

Rohini Selvaraj and D. Geraldine Bessie Amali*
School of Computer Science and Engineering, Vellore Institute of Technology, Vellore – 632014, India
Received: 21/02/2023, Accepted: 21/07/2023, Available online: 13/08/2023
*to whom all correspondence should be addressed: e-mail: geraldine.amali@vit.ac.in
https://doi.org/10.30955/gnj.004829

Graphical abstract

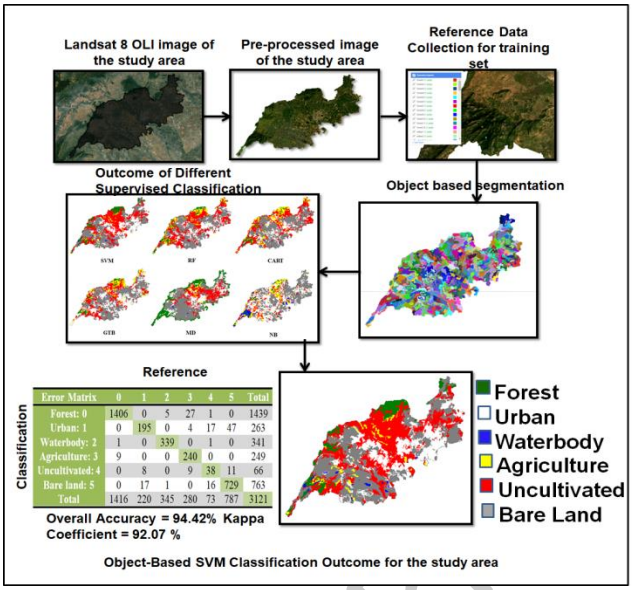

Abstract

Land Use and Land Cover (LULC) maps perform a significant part in Remote Sensing (RS) in monitoring and analyzing earth information for human development. Because of the high spectrum variability, LULC classification from RS data is extremely difficult. The study's objective is to assess the object-based LULC classification (OBC) accuracy of composite images from the Landsat 8 OLI (Operational Land Imager) and auxiliary features using SNIC segmentation and five classifiers on Google Earth Engine (GEE). The outcome of the study indicates that the OBC with only spectral features achieves lesser accuracy, because small objects on the land surface cannot be observed. But when OBC is paired with a variety of auxiliary features, the OBC may recognize small objects with greater accuracy. After many subsequent assessments the combination of the following aspect: composite image of all the seven bands, new feature set, Simple Non-Iterative Clustering (SNIC) segmentation algorithm, and Support Vector Machine (SVM) classification algorithm gives better accuracy of ~ 94.42% and kappa coefficient of 92.07. The inclusion of auxiliary feature and OBC method, reduces the misclassification rate related to the confusion of bare land, uncultivated land, and urban, which provides accurate information on forest, waterbody, and bare land classes.

Keywords: Remote sensing, land use and land cover, object-based classification, google earth engine, support vector machine

1. Introduction

Remote sensing (RS) is the technique of monitoring or collecting details about the characteristic of distant objects without physically interacting with them. RS from satellites gives important information for mapping and understanding the earth's surface. Numerous remote sensing applications are utilized potentially in various fields including agriculture, disaster management, urban studies, weather forecasting, etc. RS is letting the user access and analyzes the large temporal dataset; on the other hand, it increases the time and computational cost. In the last decade, an extensive number of RS software is developed with the features of instantaneous access, pre-processing, and web-based interfaces. Among them, Google Earth Engine (GEE) has obtained significant success as a result of providing a phenomenal cloud platform with ready-to-use remote sensing data and machine learning algorithms (Qu *et al*., 2021). Onisimo Mutanga *et al* demonstrated the power of the GEE platform in managing large data sets of various sizes and generated computerized systems for real implementation (Mutanga and Kumar, 2019). Meisam Amani *et al* briefly explain the performance of GEE for remote sensing big data applications and also discussed the trends, datasets, and application of GEE (Amani *et al*., 2020).

One of the most important remote sensing techniques is Land Use and Land Cover (LULC) classification which helps to find the regional, local, and global changes on the earth's surface. In order to monitor land degradation accurately, up-to-date LULC information is highly needed. In LULC, the term "land cover" refers to the natural and manmade characteristics that can be seen on the earth's surface, and "land use" refers to the activities that occur on the land or represent the current usage of the

property. Wetland, forest, grassland, water, and build areas are examples of land cover, whereas, for land use commercial complexes, state parks, residential residences, and tree nurseries can be taken as the examples (Fonji and Taff, 2014). Some of the most current studies based on LULC are, sand replenishment studies (Shah *et al*., 2021), farmer's perception of deforestation studies (Kouassi *et al*., 2021), land surface temperature change studies (Kafy *et al*., 2021), and classification of groundwater potentiality zone studies (Tegegne, 2022).

LULC classification research has been carried out using several pixel-based and object-based algorithms with a variety of remote sensing data such as Landsat, Sentinel, Quick Bird, Modis, and IKONOS. Pixel-based classification method classifies the individual pixels directly, whereas the object-based method first segments the pixel into objects and then classifies the individual objects. Nanki Sidhu *et al* proposed the LULC classification analysis using GEE for finding the urbanization in the study area Tuas for the years 2006-2010 (Sidhu *et al*., 2018). Pixel-based LULC classification has primarily been used for remote sensing applications, but the object-based has proven even more standard in the last ten years.M. Gholoobi *et al* compared the pixel and object-based LULC classification using the maximum likelihood algorithm (M. Gholoobi *et al*, 2010) The result of the object-based approach gives higher accuracy without any noisy outcome, although the pixel-based approach is noisy. In general, the object-oriented method delivers better results on high-resolution data, even though the use of several features for classification and higher computational cost for segmentation. Saeid Amini *et al* showed that the accuracy of the OBC method is 5.67 and 3.75 % better than the conventional Random Forest Classification (RFC) and Support Vector Machine (SVM) (Amini *et al*., 2018). Filiz Bektas Balcik *et al* proposed the OBC method of greenhouse mapping that achieved 82% and 74% accuracy with different datasets (Balcik *et al*., 2019). Connor McLaughlin *et al* showed that the use of OBC in the identification of land changes outperform compared to the other methods (McLaughlin *et al*., 2020). In both pixel and object-based classification, the accuracy depends on the certainty of data, auxiliary features, and classification algorithm.

The quality and quantity of data play a vital role in the production of object-based LULC classification. High-resolution data are important for analyzing the LULC classification in the large study area, but such a data set is limitedly available considering the financial aspect. On the other hand, medium resolution data like Landsat Thematic Mapper (TM), Multi-Spectral Scanner (MSS), and Operational Land Imager (OLI) are easily available for LULC classification. Landsat images to access the LULC classification for the different studies were effectively used by Olena Dubovyk a d *et al*(Dubovy *et al*., 2013), Kamrul Islam *et al*(Islam *et al*., 2018), Gebiaw T Ayele1*et al*(Ayele *et al*., 2018), Md. Inzamul Haque *et al*(Md. Inzamul Haque, 2017), and Gofamodimo Mashame*et al* (Mashame and Akinyemi, 2016).

Image segmentation is the next and most important step in object-based LULC classification. Segmentation divides the image into small homogenous objects based on the spectral values. A few segmentation algorithms are Multi-Scale Segmentation (MSS) (Blaschke, 2010), Simple Non-Iterative clustering (SNIC) (Yang *et al*., 2021) segmentation, and Simple Linear Iterative Clustering (SLIC) segmentation. Both SNIC and SLIC segmentation algorithms are super pixel-based clustering algorithms. SLIC algorithm clusters the pixel based on the image plan space and five-dimensional color. SNIC is an upgraded version of SLIC and it requires lesser memory space as well as faster speed (Achanta and Süsstrunk, 2017). In MSS, there is no clear relationship between the scale and the success rate. The scale of the segmentation is determined by the trial and error method. The next step of the object-based LULC classification is feature extraction. In place of feature extraction, spectral, geometric, texture, and contextual information are considered for object-based methods, whereas in traditional pixel-based methods only spectral values are used. After completing the segmentation and feature extraction steps, the data classification starts. Numerous classification algorithms are developed for LULC classification (Alshari and Gawali, 2021), e.g. MaximumLikehood (ML) classifier(Shivakumar and Rajashekararadhya, 2018), Support Vector Machine (SVM)(Wang *et al*., 2018)(Heumann, 2011), K-Nearest Neighbor (KNN)(Ban *et al*., 2010), Classification And Regression Tree (CART)(Shao and Lunetta, 2012), Random Forest (RF)(Wang *et al*., 2018), Gradient Tree Boost (GTB)(Sun *et al*., 2019), Naive Bayes (NB)(Sitthi *et al*., 2016).

The novelty and contribution of this work is the hybrid procedure combining auxiliary features (GLCM, Greay's C and some Vegetation Index) with the SNIC Segmentation algorithm applied in GEE for object-based LULC classification. In the earlier work, (Andrea Tassi *et al*., 2020) performed object-based LULC classification with GLCM and SNIC segmentation algorithm and they have achieved only 89.3% and 86.9% accuracy with the RF and the SVM classifier respectively. Compared to this earlier work, this study achieves 94.42% by adding the auxiliary features with GLCM. The important tasks of proposed OBC are listed below 1) automatic extraction of remote sensing image for object-based LULC classification; 2) data preprocessing like finding the suitable band combination of an input image and extracting the state boundary image from the raw remote sensing image; 3) partitioning the image into the multiple objects (super pixel) to be used for SNIC segmentation method. 4) identifying which auxiliary features are most suitable for object-based LULC classification; 5) comparing the performance of the SVM classifier with the other supervised classification algorithms like ML, KNN, RF, CART, GTB, and NB. The paper is structured into various sections, such as the study area, data collection and preprocessing, methodology, results and discussions, and conclusions.

2. Study area

Madurai district, that is located in the South Indian state of Tamil Nadu and has an estimated population of 1.75 million people, is selected as the study area. The city's total area, including Madurai and the Vaigai River, is 3741.73 km2. Madurai is the third-largest city in Tamil Nadu, and it is located between 90 30" and 100 30" north latitude and 770 00" and 780 30" east longitude. The study region is covered by the southeast of the Western Ghats and several mountain spurs. The climate of the study area is changeable but prominently hot and dry for eight months of the year. The difficult patterns of topography and climate build the rich biodiversity and different landscape of Madurai's LULC. To minimize the complexity of the landscape information the study area is divided into five major regions and which are forest, agricultural land, urban land, waterbody, bare land, and uncultivated land. Bare land is a piece of land on which cultivation of any crop is not possible, whereas in the Uncultivated land, the soil retains the required minerals that's go for cultivation. Figure 1 shows the location map and Landsat 8 OLI image of the study area.

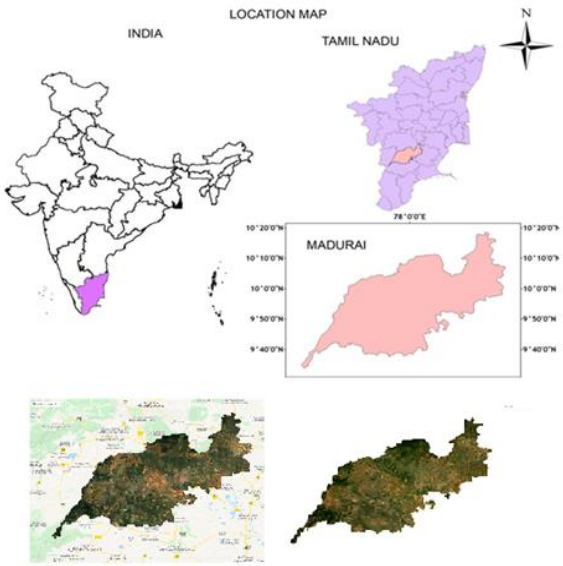

Figure 1. Location map showing the study area (Madurai) in large and Landsat 8 OLI image of the study area

3. Methodology

The study aims to determine the suitable feature set and classification algorithm for object-based LULC classification using the GEE cloud platform. Figure 2 illustrates the overall workflow of the assessment of object-based LULC classification. The workflow is a composite of six sub-processes, which are data collection, pre-processing, segmentation, feature extraction, classification, and accuracy assessment. Among the aforementioned processes, segmentation and classification are the most important process for object-based LULC classification. The GEE API is used for data collection and entire implementation (training and testing dataset creation, classification, and performance assessment). GEE works with JavaScript programming language. All these methods are processed using GEE software and processes are discussed in detail.

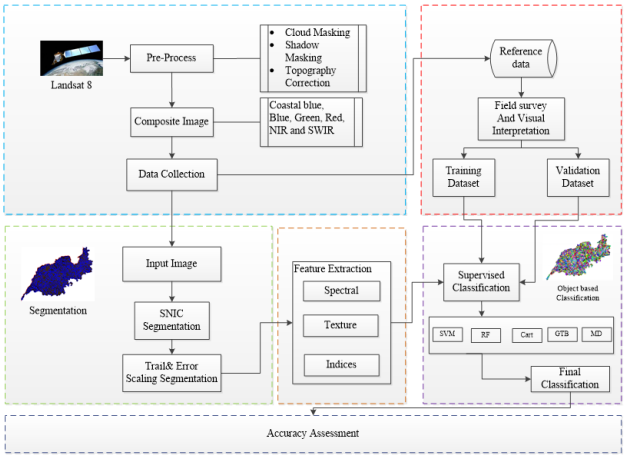

Figure 2. Flow chart for assessment of object-based LULC classification

3.1. Data collection and preprocessing

Landsat data is one of the most commonly utilized satellite datasets for LULC classification [1]. The Landsat data can be pre-processed and accessed from the GEE platform since it includes the United States Geological Survey (USGS) Landsat Operational Land Imager (OLI), Enhanced Thematic Mapper (ETM), and Thematic Mapper (TM). For this study, the 'Landsat 8 OLI Tier 1 and Level 2' atmospherically corrected and surface reflected images from 2015 are employed. It has 11 bands among them, seven bands are used for the composite, which are coastal blue, blue, green, red, Near Infrared(NIR), and Shortwave Infrared(SWIR1 and SWIR2). It consists of nine spectral bands (SR_B1-SR_B9) with 30-meter resolution excluding the panchromatic band (SR_B7: 15m resolution) and two thermal bands (SR_B10 and SR_B11) with 100-meter resolution. In Landsat 8 OLI, the sensor bands are SR_B1:costal aerosol (wavelength: 0.43-0.45 µm), SR_B2:blue (wavelength: 0.45-0.51 µm), SR_B3:green (wavelength: 0.53-0.59 µm), SR_B4:red (wavelength: 0.64-0.67 µm), SR_B5:Near InfraRed (wavelength: 0.85-0.88 µm), SR_B6:SWIR1 (wavelength: 1.57-1.65 µm), SR_B7:SWIR2 (wavelength: 2.11-2.29 µm), SR_B8:panchromatic (wavelength: 0.50-0.68 µm), SR_B9:cirrus (wavelength: 1.36-1.38 µm), SR_B10:TIRS1 (wavelength: 10.6-11.19 µm), SR_B11:TIRS2 (wavelength: 11.50-12.51 µm). To create cloud-free composite images, the image synthesis and cloud mask approaches are used. The composite image is filtered with the geographical boundary conditions of the study area.

3.2. Segmentation

Image segmentation, the first step in object-based LULC classification, separates the image into homogenous and discrete objects depends on the object's colour, spectral characteristics, uniform texture, and shape. The SNIC segmentation algorithm is used in this study. It is one of the most dominant segmentation algorithms that use the general grid to make the k-centroids in the image plane. Based on the initial k-centroids, the size of the super pixels is determined from equation 1,

$$s = \sqrt{N / K} \quad (1)$$

where N is how many pixels there are in the picture and K is the initial centroids. SNIC segmentation algorithm proceeds based on the super-pixel label, color, spatial position, and distance from the super-pixel centroid to the prospective pixel. These K elements are used to form a priority queue Q. Whenever Q is not empty, it always picks the element with the shortest distance. If the pixel has not yet been labeled, a new element is produced for each linked neighbor pixel of the popped element, and the distance from the connected centroid and the label of the connected centroid is assigned to it. The item is then placed in the queue and then an additional element added to the queue is used to update the related centroid value in real-time. The SNIC algorithm ends when all of the image's pixels have been tagged and Q has been emptied.

In the GEE tool, the SNIC segmentation input arguments are the input images for segmentation, size of seed location for gridding, compactness, connectivity, neighborhood size, and seed30. The segmentation input argument 'Size' determines the segmented object size and it is finalized according to the trial-and-error method, in addition to subjective perception. The default seed size is 5, however, the size does not give a better result for the input image. The seed size is linearly incremented and tested for the performance of the segmentation. Finally, the seed size 10 gives better segmentation than the other seed size segmentation. In this study, input arguments are set as follow: Size= 10, Compactness = 5, Connectivity = 8 and Neighborhood Size = 256. The SNIC segmentation outcomes from GEE are shown in Figure 3.

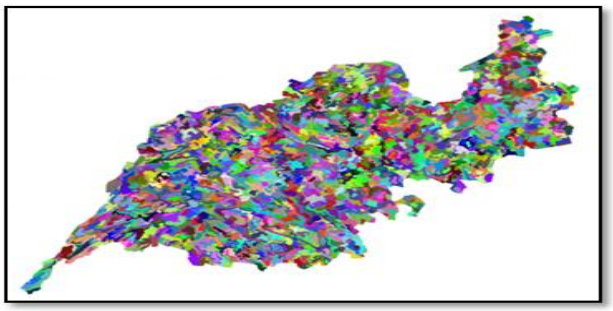

Figure 3. SNIC segmentation for the study area

3.3. Feature extraction and feature set creation

Image segmentation allows the extraction of features associated with image objects. Finding the appropriate auxiliary feature for object-based LULC classification is one of the main processes in the current study. The feature set is selected based on the performance analysis of LULC classification. In this study, a few spectral features, texture features, indices, and spatial correlation are investigated. For spectral feature, the mean of all the seven-band, mean of false-color composite bands, and spectral entropy are used. Texture features are extracted using entropy, GLCM, and Gearys C-correlation. Frequently used remote sensing indices, that are NDVI(Normalized Difference Vegetation Index), EVI(Enhanced Vegetation Index), DVI(Difference Vegetation Index), and RVI (Ratio Vegetation Index)are employed. The feature set selection method is implemented and tested in the GEE platform using the SVM classification algorithm. Table 1 shows the details of the extracted features with band descriptions. Among all of the above features mean of all seven bands, GLCM (Entropy), Grearys C-correlation, entropy, and NDVI texture feature set gives a better result.

Table 1. The details of the extracted features with band combinations

Category	Feature	Description
Spectral	F1: mean of all seven bands	Mean('SR_B4', 'SR_B3', 'SR_B2', 'SR_B5','SR_B1','SR_B6', 'SR_B7')
	F2: mean of false-color urban composite	Mean('SR_B7', 'SR_B6', 'SR_B4')
	F3: mean of natural color composite	Mean('SR_B4' , 'SR_B3', SR_B2')
	F4: mean of natural with atmospheric removal composite	Mean('SR_B7', 'SR_B5', 'SR_B3')
Texture	F5: GLCM	Angular Second Moment (GLCM_ASM), Energy, (inertia moment), Correlation, Entropy, and the Inverse Difference Moment
	F6: ENTROPY	Entropy ('SR_B2')
	F7: NDTX	Texture of NDVI ('SR_B5',' SR_B4')
	F8: Geary's C	Measure of spatial association
Indices	F9:RVI	('SR_B5')/('SR_B4')
	F10:EVI	'2.5 * (('SR_B5' – 'SR_B4') / ('SR_B5' + 6 * 'SR_B4'- 7.5 * 'SR_B2' + 1)
	F11:DVI	('SR_B5')-('SR_B4')
	F12:NDVI	('SR_B5')-('SR_B4')/ ('SR_B5')+('SR_B4')

3.4. Reference data

The reference datasets are utilized to generate ROI (region of interest) polygons on the Landsat data in GEE software, which is used to generate the training regions and testing regions. For training and testing, a total of 83 polygons are used for classification and the pixel count of

each polygon is approximately (1500-2500 pixels). The collected reference data are randomly separated by 70:30 percentages for training and testing and then the same set of data is used for validation assessment of the confusion matrix. To create the ground truth points, the polygon is overlaid with the Google Earth high-resolution base map and manually labeled each polygon as agricultural land, uncultivated land, forest, bare land, water body, and urban land type. Known ground truth points (training and validation) are may create spatial autocorrelation. Remove samples that are quite close to any other sample in order to rule out samples that could be associated in this way (s). Spatial joins can be used to achieve this.

3.5. Object-based lulc classification

The specific objective of this research is to compare the performance of the SVM classifier with other supervised classification algorithms. Here SVM, CART, RF, ML, RTB, and NB supervise classification algorithms are employed to find the object-based LULC classification (Adepoju K.A. and Adelabu S.A, 2020). Compared with SVM, in deep learning the training complexity is more for handling the hyperspectral data. Due to this difficulty, SVM is not compared with other deep learning methods. Some linear supervised machine learning algorithms normally require multicollinearity reduction and feature normalization. In a regression model, multicollinearity occurs when more than two independent variables are significantly associated with one another. Because of their deterministic support vector solutions, support vector machines may not suffer from multicollinearity. The study implements the SVM algorithm with the least absolute shrinkage to avoid multicollinearity. The arguments of the SVM Classifier are SVM type (C_SVM), shrinkage (1), and kernel type (Linear). The argument of RF is the number of trees (20). The arguments of the cart are maxnodes (10) and min leaf population (1). The arguments of GTB are the number of trees (20), shrinkage(0.1), and sampling rate(1). The arguments of MD are metric (Euclidean), kNearest (5). The argument of NB classifier is lambda(0.1). The arguments of the classifier are chosen by trial and error method based on the accuracy assessment. All the classification processes are performed in GEE using the above set of supervised classification algorithms. To implement the object-based LULC classification, the code requires a set of information like region of interest, class information, training data set, and testing dataset. In the study area, LULC classes mostly cover agricultural land, uncultivated land, forest, bare land, water body, and urban land type. Hence, the six-class training dataset is created using the GEE interface and the data points are imputed as polygons. For each class, more than 20 polygons are created, and to improve the supervised classification information, some buffer data points are created for each class.

4. Result and discussion

4.1. Assessment of band combination

In the assessment of band combinations, different false-color combinations and all seven band combinations are compared. As a result, the final working band combination is a composite of seven bands that gives better results than the other composites and these specific combinations are chosen from the literature (Hütt *et al*., 2016).

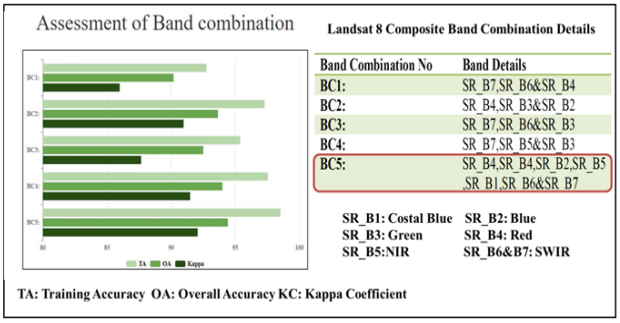

Figure 4. Assessment of different band combinations for object-based LULC classification

Landsat 8 band combination details and accuracy assessment for the band combination are shown in Figure 4. The SVM classification algorithm is used for the assessment of band combinations. BC1 is a combination of SWIR and the red band and it gives the false-color urban composite. BC1 composite shows vegetation in various tones of green. Denser vegetation is represented by deeper colors of green, whilst minimal vegetation is represented by lighter tones. The color of urban areas is blue, whereas soils are varying degrees of brown. Compared to that of other band combinations, the overall accuracy of the BC1 is very low. BC2 is a natural color composite combination of the red, blue, and green bands. In BC2, healthy vegetation is green, but unhealthy vegetation is shown as brown. Water appears dark blue or black, whereas the urban areas seem white and grey. The accuracy of the BC2 is affected because not much difference between the classes of uncultivated land and bare land is noticed. BC3 is a combination of SWIR and green bands and the combination gives lower accuracy for the urban classes. BC4 is natural with an atmospheric removal color composite combination of SWIR1, NIR, and green bands. BC5 is the combination of all seven bands that give a false-color composite. In BC5, the composite image is very near to what normal human eyes can observe. In comparison to the other band combinations, BC5 gives a better result for object-based LULC classification.

4.2. Selection of auxiliary feature

The selection of appropriate features is the most important part of an object-based LULC classification. Figure 5 shows the feature set combination details and assessment of the different feature sets. FC1 exhibits spectral features of the study area and it is calculated from the mean of all seven bands. The overall accuracy of FC1 is 93.8%. For the next feature set FC2 spectral and texture, features are combined. GLCM entropy is used for the texture feature and the FC2 combination is achieved about 94% of overall accuracy. In the next feature set FC3, GLCM_ASM is added with the FC2 feature set. But this feature set reduces the overall accuracy by 0.1 %

compared with the previous feature set. The FC4 feature set is a combination of spectral features, texture features, and indices. For indices, EVI is used and the present combination provides 87.7% overall accuracy. A considerable percentage of accuracy is reduced because of the EVI feature, as a result of IDM feature is added with the FC2 feature set. The overall accuracy of FC5 and FC6 is 93.6% and 92.6% respectively. Entropy with the FC2 feature set achieves the new highest accuracy of 94.1%. The aforementioned feature set is FC7 and this feature set creates a new breakpoint. The FC8 feature set is the combination of NDVI texture with the FC7 feature set and this feature set improves the accuracy by 94.27%. Among the above feature sets, the mean of all seven bands, GLCM(Entropy), Grearys C-correlation, entropy, and NDVI texture feature set (FC9) gives a better result. The average spectral signature of all LULC classes concerning the selected feature set is explained in Figure 6, which demonstrates the effect of the spectral band for specific classes. For example, the impact of the red band in the forest class is low compared to the uncultivated class.

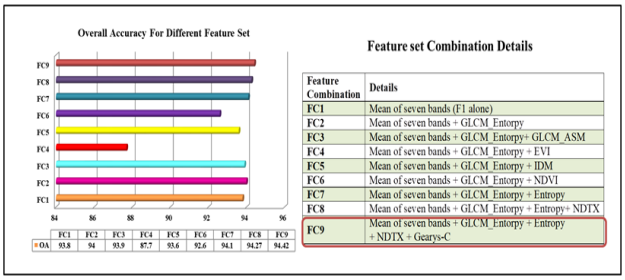

Figure 5. The assessment of different feature sets combinations for object-based LULC classification

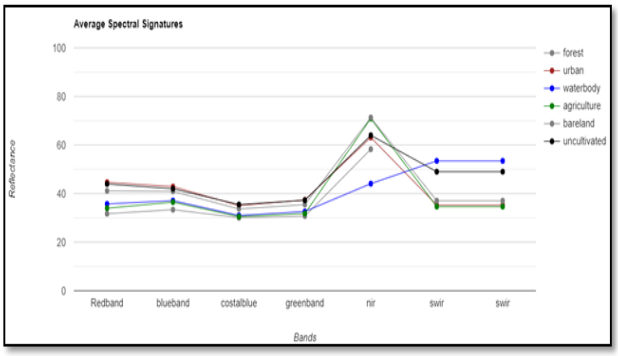

Figure 6. Average Spectral Signature of LULC classes for the selected auxiliary feature set

4.3. Assessment of object-based supervised classification

The accuracy of different object-based supervised classifications is investigated in this study using the error matrix with validation samples. The outcome of object-based LULC Classification for various supervised classification methods is shown in Figures 7 and 8.

Among the various classifiers used in the study, SVM and RF provide better results for LULC classification obtaining results with comparable accuracy. NB classifier shows a very low overall accuracy compared with the other classification.

The error matrix of the SVM classifier and sample LULC classification result is shown in Figure 9. The error matrix of the SVM classifier is evident that there are misclassifications between the classes. The majority of the misclassification happened between bare land class, uncultivated land class, and urban land class. Misclassification is rarely present in the water body and forest classes. In this study, the term accuracy refers to the ratio of the correctly predicted land class to the total predicted class. Other performance metrics like precision and recall are used, but they are mentioned in different terms like recall as producer accuracy and precision as user accuracy. The class-wise user accuracy and producer accuracy are as follows: UA: [0:0.9929, 1: 0.8863, 2: 0.9826, 3: 0.8571, 4: 0.5205, 5: 0.9263], PA: [0: 0.9770, 1: 0.7414, 2: 0.9941, 3: 0.9638, 4: 0.5757, 5: 0.9554] .

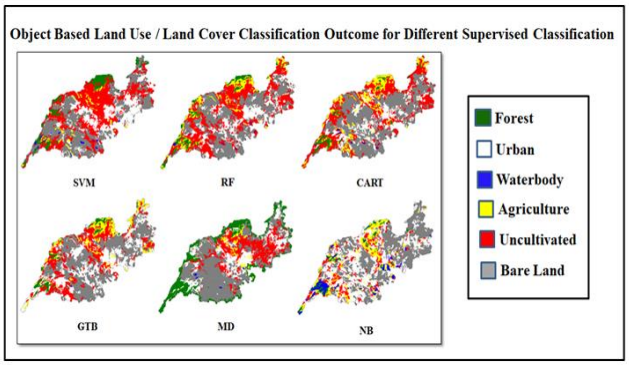

Figure 7. Object-based LULC classification outcome for different supervised classification

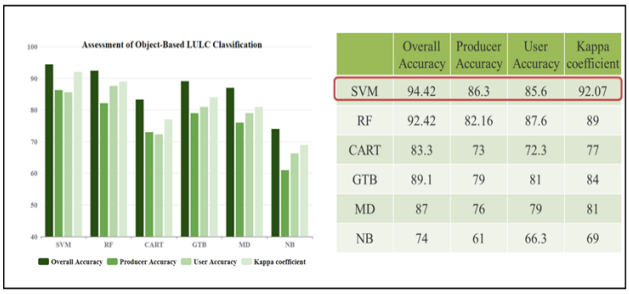

	Overall Accuracy	Producer Accuracy	User Accuracy	Kappa coefficient
SVM	94.42	86.3	85.6	92.07
RF	92.42	82.16	87.6	89
CART	83.3	73	72.3	77
GTB	89.1	79	81	84
MD	87	76	79	81
NB	74	61	66.3	69

Figure 8. Assessment of different supervised classifications for object-based LULC classification

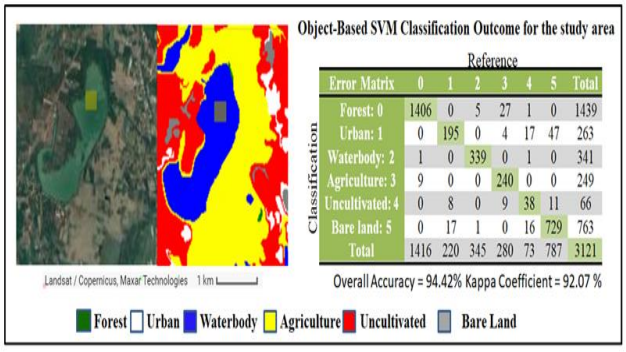

Figure 9. LULC classification result and error matrix for SVM classifier

The area distribution of the study area is presented in Figure 10. Among the various LULC classes, the water class covers only 66.820 km2 and the next lowest distribution is the forest class 265.52 km2. In the total study area, 66.71 % of the land is covered by the uncultivated class (1038.933 km2) and bare land class (1422.76 km2). LULC

area distribution of urban and agriculture classes is 534.41 km2, and 367.65 km2 respectively.

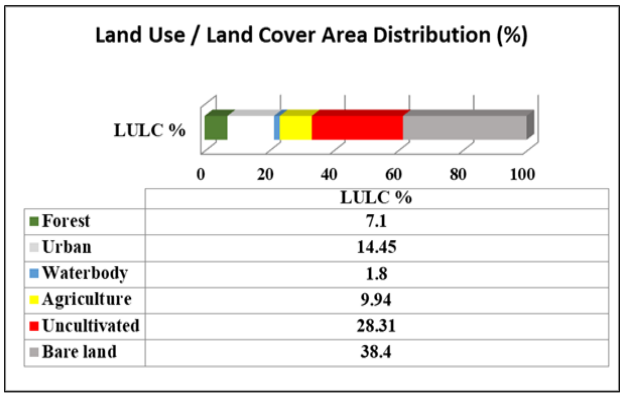

	LULC %
Forest	7.1
Urban	14.45
Waterbody	1.8
Agriculture	9.94
Uncultivated	28.31
Bare land	38.4

Figure 10. Land Use and Land Cover area distribution

5. Conclusion

The accurate mapping of LULC is extremely helpful for many environmental applications like urban planning, land rehabilitation, land management, and risk analysis. The objective of this research was to assess the land distribution of the study area using the object-based LULC classification method and demonstrated how the GEE platform supported the analysis by providing a user-friendly interface. The results of this research can be summarized as follows: (i) feature set was selected based on the performance analysis of different feature sets; (ii) the accuracy of different object-based supervised classification results was investigated (iii) the area distribution of the study area is calculated. Within the GEE tool, this work implemented and tested an OBC method using the SNIC algorithm to create spatial clusters. As the accuracy of the classification varied continuously, it depends on the different features, composite imageries, and classification algorithms. Therefore, the single feature set or the single classification algorithm may not be optimal for all LULC classification problems. Accordingly, for this study area, the set of features and classification algorithms gives an improved outcome with an overall accuracy of 94.42% and kappa coefficient of 92.07. Further, the work could be expanded by adding annual temporal data for LULC change detection to find the annual land degradation report.

Data availability statement

Landsat 8 OLI Data was taken from the Google Earth Engine Data Catalog (Landsat-8 image courtesy of the U.S. Geological Survey). The Google Earth Engine script, reference data, and LULC outputs may be made available on request from the authors.

References

Achanta R. and Süsstrunk S. (2017). Superpixels and polygons using simple non-iterative clustering. Proceedings - 30th IEEE Conference on Computer Vision and Pattern Recognition, CVPR 2017, 2017-Janua (Ic), 4895–4904. https://doi.org/10.1109/CVPR.2017.520

Adepoju K.A. and Adelabu S.A. (2020). Improving accuracy evaluation of Landsat-8 OLI using image composite and multisource data with Google Earth Engine. *Remote Sensing Letters*, **11**(2), 107–116. https://doi.org/10.1080/2150704X.2019.1690792

Alshari E.A. and Gawali B.W. (2021). Development of classification system for LULC using remote sensing and GIS. *Global Transitions Proceedings*, **2**(1), 8–17. https://doi.org/10.1016/j.gltp.2021.01.002

Amini S., Homayouni S., Safari A. and Darvishsefat A.A. (2018). Object-based classification of hyperspectral data using Random Forest algorithm. *Geo-Spatial Information Science*, **21**(2), 127–138. https://doi.org/10.1080/10095020.2017.1399674

Ayele G., Tebeje A.K., Demissie S., Belete M., Jemberie M., Dereje T. and Teshale E. (2018). Time series land cover mapping and change detection analysis using geographic information system and remote sensing, Northern Ethiopia. *Air, Soil and Water Research*, **11**, 1–18. https://doi.org/10.1177/1178622117751603

Balcik F.B., Senel G. and Goksel C. (2019). Greenhouse mapping using object based classification and sentinel-2 satellite imagery. 2019 8th International Conference on Agro-Geoinformatics, *Agro-Geoinformatics* 2019, June 2015, 2–6. https://doi.org/10.1109/Agro-Geoinformatics.2019.8820252

Ban Y., Hu H. and Rangel I.M. (2010). Fusion of Quickbird MS and RADARSAT SAR data for urban land-cover mapping: Object-based and knowledge-based approach. *International Journal of Remote Sensing*, **31**(6), 1391–1410. https://doi.org/10.1080/01431160903475415

Blaschke T. (2010). Object based image analysis for remote sensing. *ISPRS Journal of Photogrammetry and Remote Sensing*, **65**(1), 2–16. https://doi.org/10.1016/j.isprsjprs.2009.06.004

Fonji S.F. and Taff G.N. (2014). Using satellite data to monitor land-use land-cover change in North-eastern Latvia. *SpringerPlus*, **3**(1), 1–15. https://doi.org/10.1186/2193-1801-3-61

Gholoobi M., Tayyebib A., Taleyi M. and Tayyebi A.H. (2010). Comparing pixel based and object based approaches in land use classification in mountainous areas. International Archives of the Photogrammetry, *Remote Sensing and Spatial Information Sciences - ISPRS Archives*, XXXVIII(2), 573–581. https://doi.org/10.1109/JBHI.2016.2515993

Heumann B.W. (2011). An object-based classification of mangroves using a hybrid decision tree-support vector machine approach. *Remote Sensing*, **3**(11), 2440–2460. https://doi.org/10.3390/rs3112440

Islam K., Jashimuddin M., Nath B. and Nath T.K. (2018). Land use classification and change detection by using multi-temporal remotely sensed imagery: The case of Chunati wildlife sanctuary, Bangladesh. *Egyptian Journal of Remote Sensing and Space Science*, **21**(1), 37–47. https://doi.org/10.1016/j.ejrs.2016.12.005

Jin Y., Liu X., Yao J., Zhang X. and Zhang H. (2020). Mapping the annual dynamics of cultivated land in typical area of the Middle-lower Yangtze plain using long time-series of Landsat images based on Google Earth Engine. *International Journal of Remote Sensing*, **41**(4), 1625–1644. https://doi.org/10.1080/01431161.2019.1673917

Kouassi J.L., Gyau A., Diby L., Bene Y. and Kouamé C. (2021). Assessing land use and land cover change and farmers' perceptions of deforestation and land degradation in south-west Côte d'Ivoire, West Africa. Land, 10(4). https://doi.org/10.3390/land10040429

Mashame G. and Akinyemi F. (2016). Towards a remote sensing based assessment of land susceptibility to degradation: examining seasonal variation in land use-land cover for modelling land degradation in a semi-arid context. ISPRS Annals of the Photogrammetry, Remote Sensing and Spatial Information Sciences, 3(July), 137–144. https://doi.org/10.5194/isprs-annals-III-8-137-2016

McLaughlin C., Woodley A., Geva S., Chappell T., Kelly W., Boles W., De Vine L. and Hutson H. (2020). Object Based Remote Sensing Using Sentinel Data. 2020 Digital Image Computing: Techniques and Applications, DICTA 2020. https://doi.org/10.1109/DICTA51227.2020.9363427

Md. Inzamul Haque R.B.D. (2017). Land cover change detection using GIS and remote sensing techniques: A spatio-temporal study on Tanguar Haor, Sunamganj, Bangladesh. *The Egyptian Journal of Remote Sensing and Space Sciences Journal*, **3**, 417–451. https://doi.org/10.1201/b19321

Mutanga O. and Kumar L. (2019). Google earth engine applications. *Remote Sensing*, **11**(5), 11–14. https://doi.org/10.3390/rs11050591

Olena D., Gunter M., Christopher C. and Thonfeld F.K. (2013). Object-based identification of vegetation cover decline in irrigated agro-ecosystems in Uzbekistan. *Quaternary International*, **311**, 163–174. https://doi.org/10.1016/j.quaint.2013.07.043

Qu L., Chen Z., Li M., Zhi J. and Wang H. (2021). Accuracy improvements to pixel-based and object-based LULC classification with auxiliary datasets from google earth engine. *Remote Sensing*, **13**(3), 453. https://doi.org/10.3390/rs13030453

Shah A.K., Morya J. and Majethiya H.V. (2021). Application of Land-Use Land-Cover Map for Sand Replenishment Study: A case study of Orsang River , Gujarat. February 2022, 17–25.

Shao Y. and Lunetta R.S. (2012). Comparison of support vector machine, neural network, and CART algorithms for the land-cover classification using limited training data points. *ISPRS Journal of Photogrammetry and Remote Sensing*, **70**, 78–87. https://doi.org/10.1016/j.isprsjprs.2012.04.001

Shivakumar B.R. and Rajashekararadhya S.V. (2018). Investigation on land cover mapping capability of maximum likelihood classifier: A case study on North Canara, India. *Procedia Computer Science*, **143**, 579–586. https://doi.org/10.1016/j.procs.2018.10.434

Sidhu N., Pebesma E. and Câmara G. (2018). Using Google Earth Engine to detect land cover change: Singapore as a use case. *European Journal of Remote Sensing*, **51**(1), 486–500. https://doi.org/10.1080/22797254.2018.1451782

Sitthi A., Nagai M., Dailey M. and Ninsawat S. (2016). Exploring land use and land cover of geotagged social-sensing images using naive bayes classifier. *Sustainability* (*Switzerland*), **8**(9), 921. https://doi.org/10.3390/su8090921

Sun F., Wang R., Wan B., Su Y., Guo Q., Huang Y. and Wu X. (2019). Efficiency of extreme gradient boosting for imbalanced land cover classification using an extended margin and disagreement performance. *ISPRS International Journal of Geo-Information*, **8**(7), 0315. https://doi.org/10.3390/ijgi8070315

Tassi A. and Vizzari M. (2020). Object-Oriented LULC Classification in Google Earth Learning Algorithms. *Remote Sensing*, **12**, 1–17. doi:10.3390/rs12223776

Tegegne A.M. (2022). Applications of Convolutional Neural Network for Classification of Land Cover and Groundwater Potentiality Zones. *Journal of Engineering* (*United Kingdom*), 2022. https://doi.org/10.1155/2022/6372089

Wang X., Liu S., Du P., Liang H., Xia J. and Li Y. (2018). Object-based change detection in urban areas from high spatial resolution images based on multiple features and ensemble learning. *Remote Sensing*, **10**(2), 276. https://doi.org/10.3390/rs10020276

Yang L., Wang L., Abubakar G.A. and Huang J. (2021). High-resolution rice mapping based on snic segmentation and multi-source remote sensing images. *Remote Sensing*, **13**(6), 1148. https://doi.org/10.3390/rs13061148